DOI 10.1007/s11094-018-1835-0
Pharmaceutical Chemistry Journal, Vol. 52, No. 5, August, 2018 (Russian Original Vol. 52, No. 5, May, 2018)

MICROWAVE-ASSISTED SYNTHESIS, *IN VIVO* ANTI-INFLAMMATORY AND *IN VITRO* ANTI-OXIDANT ACTIVITIES, AND MOLECULAR DOCKING STUDY OF NEW SUBSTITUTED SCHIFF BASE DERIVATIVES

Muhammad Hanif,[2] Mubashir Hassan,[1] Muhammad Rafiq,[1,3] Qamar Abbas,[4] Ansa Ishaq,[5] Saba Shahzadi,[6,7] Sung-Yum Seo,[2] and Muhammad Saleem[8,*]

Original article submitted November 21, 2017.

In view of considerable interest in the design and synthesis of new heterocyclic compounds with promising biological activities for medical and biological applications, a series of eight imine derivatives have been synthesized through microwave-assisted Schiff base formation by reacting 2-(4-methoxyphenyl)acetohydrazide **(3)** and 4-amino-3-(4-methoxybenzyl)-1H-1,2,4-triazole-5(4H)-thione **(6)** with various substituted aldehydes. Structures of the newly synthesized compounds were characterized by FT-IR, ^{1}H NMR and ^{13}C NMR spectral analysis. All the synthesized derivatives were screened for their *in vivo* anti-inflammatory and *in vitro* anti-oxidant activities using carrageenan induced rat paw edema test and DPPH free radical scavenging assay, respectively. In addition, molecular docking experiment was also performed to check the actual binding affinity of ligand against target protein. Compounds **4a**, **4c**, **7a,** and **7c** screened as potent anti-inflammatory drugs significantly lowered the volume of rat paw edema ($P < 0.05$). In case of anti-oxidant assay, compound **7a** with ferrocenyl group as substituent R and 3,4-disubstitued 1,2,4-triazole as side coupled group exhibited IC_{50} value of 7.2 ± 2.7 μg/mL comparable with that of the reference ascorbic acid (2.61 ± 0.29 μg/mL) and was the most active compound among the series. However, no prominent results were obtained in case of aralkanoic acid hydrazide substituted Schiff base derivatives **4a – 4d**. It is believed that the synthesized Schiff base derivatives can be used for the development of potent anti-inflammatory and anti-oxidant drugs with considerable advantages of convenient synthetic strategy possessing high product yield, short reaction time, and convenient handling. The molecular docking results were found in good correlation with experimental IC_{50} values.

Keywords: microwave assisted synthesis; Schiff base derivatives; *in vivo* anti-inflammatory activity; *in vitro* anti-oxidant activity.

1. INTRODUCTION

Inflammation is a physiological reaction to injury and infectious, allergic, or chemical irritation. Inflammatory processes are complex biochemical phenomena characterized by tissue edema, pain, and leukocyte infiltration [1]. To evaluate the anti-inflammatory activity of test samples, various types of anti-inflammatory assays such as carrageenan induced paw edema, serotonin induced paw edema, cotton pellet induced granuloma formation, peritoneal capillary permeability test, and ethyl phenyl propionate or arachidonic acid induced ear edema are usually employed. Among all the inflammatory tests, the most extensively used test for the screening of new anti-inflammatory drugs is the carrageenan induced paw edema in rat [2]. Inflammation is a part of complex biological response for vascular tissues and mediators involved in the inflammation reaction which can maintain, induce, or aggravate many diseases. Steroidal or non-stero-

[1] Department of Chemistry, Government College University, Faisalabad (Sub-Campus Layyah), Pakistan.
[2] College of Natural Sciences, Department of Biology, Kongju National University, Gongju, Chungcheongnam 32588, Republic of Korea.
[3] Department of Biochemistry and Biotechnology (Baghdad-ul-Jadeed Campus), The Islamia University of Bahawalpur 63100, Pakistan.
[4] Department of Physiology, University of Sindh, Jamshoro 76080, Pakistan.
[5] Department of Chemistry, University of Sargodha (Sub-Campus Mianwali), Pakistan.
[6] Department of Bioinformatics, Virtual University (Davis Road Campus), Lahore, Pakistan.
[7] Institute of Molecular Science and Bioinformatics, 28 Nisbet Road, Opt. Dyal Singh Trust Library, Lahore 54000, Pakistan.
[8] Department of Chemistry, University of Sargodha, sub-campus Bhakkar.
* e-mail: saleemqau@gmail.com

idal chemical therapies are the current treatment for inflammatory disorders. Pain is the most prevalent inflammatory symptom, and the two severe forms of inflammatory pain are osteoarthritis (OA) and rheumatoid arthritis (RA). For treating pain and inflammation, nonsteroidal anti-inflammatory drugs (NSAIDs) are used worldwide, which inhibit cyclooxygenase-1 (COX-1) and cyclooxygenase-2 (COX-2) enzymes [3, 4].

Total phenolics, total anthocyanins, total flavonoids, total triterpenes, and monomeric compounds have been reported as anti-oxidant and anti-inflammatory agents [5]. Recently, Brazilian red propolis and its bioactive compounds such as vestitol and neovestitol have been reported to possess anti-inflammatory and antimicrobial activity [6]. Bleeding and gastrointestinal tract (GIT) erosions are two major side effects of NSAIDs, which have been observed even at low doses of aspirin. In this regard, hybrid prodrugs NO-NSAIDs have been reported [7]. Calcineurin (CN) inhibitors such as tacrolimus and cyclosporine A (CsA) possess potent anti-inflammatory and immunosuppressive properties and have been reported as beneficial treatment for autoimmune and inflammation diseases, but these drugs also exhibit severe nephrotoxicity and hepatotoxicity side effects [8]. Norartocarpetin and mornigrol D obtained from *M. nigra* root bark inhibit the release of β-glucuronidase from rat polymorphonuclear leucocytes and show potent anti-inflammatory activity [9, 10]. Several studies showed the effect of various types of "berries" such as strawberry, blueberry and chokeberry as anti-inflammatory agents [11]. Hence, over the last century, inflammation remains the topic of numerous studies at the cellular and molecular level. As of today, several mediators that can modulate, initiate, and reduce inflammation have been identified. More recently, several novel specialized pro-resolving mediators (SPMs) have identified [12].

The term antioxidant is applied in medicine and nutrition to substances with low concentration levels that reduce reactive nitrogen species (RNS) or reactive oxygen species (ROS) before they can oxidize other molecules [13]. A growing amount of evidence has been accumulated indicating the role of ROS such as singlet oxygen (1O2), superoxide anion ($O2^{\bullet-}$), peroxyl radicals ($ROO^{\bullet}$), and hydroxyl radical ($HO^{\bullet}$) in the pathophysiology of aging and various degenerative diseases [14]. Among the cellular and extracellular components, proteins, enzymes, and lipids, RNA and DNA are the major targets for these reactive species. The antioxidative effect is mainly due to phenolic components, such as phenolic acids, flavonoids and phenolic diterpenes [15]. In addition to their role as antioxidants, these compounds exhibit a wide spectrum of medicinal properties, such as anti-allergic, anti-inflammatory, anti-microbial, anti-thrombotic, cardioprotective, and vasodilatory effects [16]. Living cells possess protective enzymatic and non-enzymatic defense systems of antioxidants that suppress excess production and enables inactivation of ROS. However, aging and various external factors such as alcohol, smoke, diet, and some drugs decrease the capability of such protective systems. In addition, ROS induce lipid peroxidation causing the deterioration of foods, which induces the oxidation of lipids and DNA resulting in membrane damage, increased membrane fluidity, and changes that lead to cancer via DNA mutation [14, 17]. Antioxidant-based drug formulations are increasingly being recommended because they act directly upon oxidative processes and are used for the prevention and treatment of complex diseases such as stroke, atherosclerosis, Alzheimer's disease, diabetes, cancer, and health problems related to aging [18]. Hydroxy-substituted Schiff bases have been reported as good free-radical scavenging agents [19]. Metal complexes containing 2,6-di-*tert*-butylphenol group have been reported as anti-oxidant, anti-inflammatory and ROS scavenging agents [20]. Oxidative stress is thought to result from imbalance between the free radicals and ROS and the antioxidants that scavenge them [21].

Herein, we report the microwave-assisted synthesis of novel Schiff base derivatives and their *in vivo* anti-inflammatory activity using carrageenan induced rat paw edema test as well as *in vitro* anti-oxidant activity employing DPPH free-radical scavenging assay. Compounds **4a**, **4c**, **7a,** and **7c** significantly lower the volume of rat paw edema ($P < 0.05$) when screened as potent anti-inflammatory drugs among the series, while one of the synthesized compounds (**7a)** with ferrocenyl group as substituent R and 3,4-disubstitued 1,2,4-triazole as side coupled group exhibited IC_{50} value of 7.2 ± 2.7 μg/mL comparable with that of reference ascorbic acid (2.61 ± 0.29 μg/mL) and was the most active compound among this series. In addition, computational experiment was performed to check for significant binding of these compounds with COX-1 and COX-2. The molecular docking results were found in good correlation with experimental IC_{50} values.

Recently, Yehye, et al. [22] reported on triazole Schiff base derivatives and evaluated their anti-oxidant activity. Several aralkyl and alkoxy phenyl moieties were hybridized to the triazole skeleton via imine linkage. Among the synthesized materials, a Schiff base containing the phenyl group substituted with tertiary butyl and hydroxyl unit was found to possess highest biological activity with IC_{50} of 46.13 ± 0.31 μM [22]. Our synthesized compounds exhibited bicyclo, ferocenyl, or bithiophenyl units connected to the central triazole skeleton through imine linkage. The most potent compound contained a ferocenyl unit hybridized to the triazole skeleton with biological activity ($IC_{50} = 7.2 \pm 2.7$ μM) about six times better than that of reported material [22] and much more close to the reference drug ascorbic acid. In addition, we have studied the synthesized compounds for molecular docking in order to better evaluate the drug binding modes. We believe that the presented data will be useful for the future investigation and development of bioactive compounds.

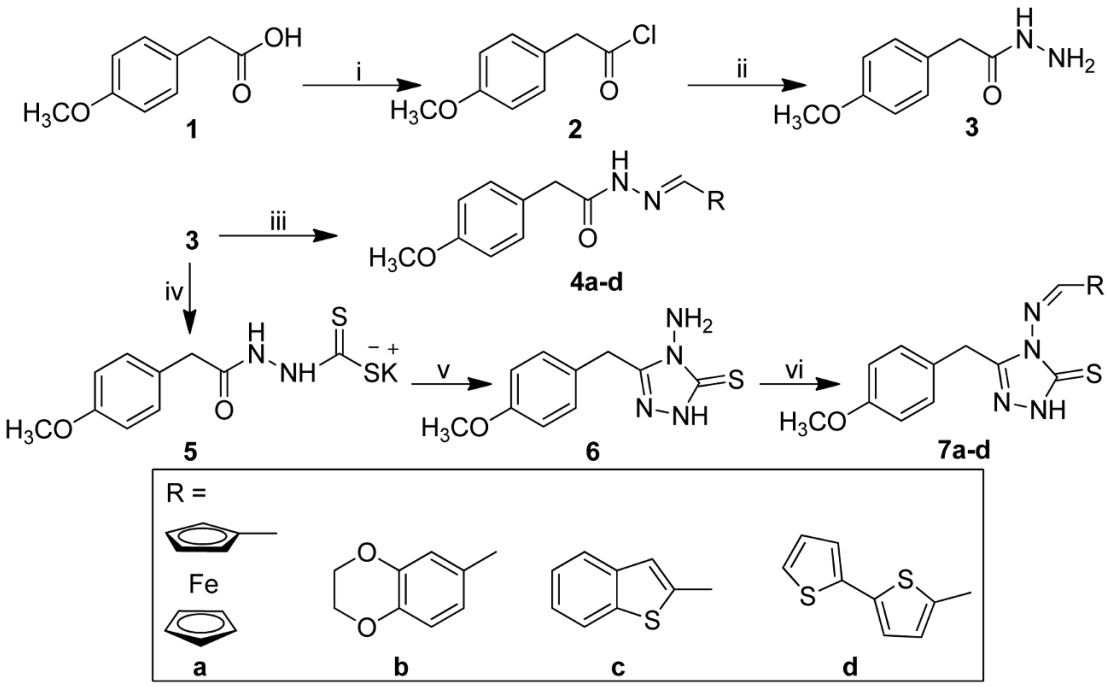

Scheme 1. Synthesis of Schiff base derivatives **4a – 4d** and **7a – 7d**. Reagents and conditions: (i) $POCl_3$, $ClCH_2CH_2Cl$, reflux 3 h; (ii) hydrazine hydrate, TEA, MeCN, reflux 3 h; (iii) various substituted aldehydes, methanol, microwave pulses (10 min); (iv) CS_2, KOH, methanol, stirring at 0°C, 1 h; (v) hydrazine hydrate (80 %), water, reflux, 10 – 12 h; (vi) various substituted aldehydes, methanol, microwave pulses (10 min).

2. EXPERIMENTAL

2.1. Materials and Methods

Substrate and reagents. 2-(4-Methoxyphenyl) acetic acid, ferrocenecarboxaldehyde, 2,3-dihydrobenzo[*b*]dioxine-6-carbaldehyde, benzo[*b*]thiophene-2-carbaldehyde, [2,2′-bithiophene]-5-carbaldehyde and phosphorous oxychloride were purchased from Aldrich. Hydrazine hydrate (80%), TEA, CS_2, KOH, sodium hydrogen carbonate (Sigma-Aldrich); ethanol, methanol, chloroform, water, acetonitrile, dimethyl sulfoxide, petroleum ether, ethyl acetate, *n*-hexane (Samchun Chemicals, Korea); and H_2SO_4, HCl (Jin Chemical & Pharmaceutical Co. Ltd., Korea) were used in experiments.

Analytical instrumentation. The reaction progress was monitored by thin layer chromatography (TLC) and the R_f values were determined by employing pre–coated silica gel aluminum plates Kieselgel 60 F_{254} from Merck (Germany). TLC patterns were visualized under a UV lamp (VL–4 LC, France). The melting points (MPs) were determined using a Fisher Scientific (USA) melting point apparatus and remained uncorrected. The IR spectra were recorded in KBr pellets on a Shimadzu FTIR–8400S spectrophotometer (Kyoto, Japan). Proton and carbon nuclear magnetic resonance (^{1}H NMR and ^{13}C NMR) spectra were recorded on a Bruker Avance 400 MHz spectrometer with TMS as the internal standard. The chemical shifts are reported as δ values (ppm) measured downfield from the internal standard tetramethylsilane in the indicated organic solution. Peak multiplicities are denoted as follows: s, singlet; d, doublet; m, multiplet. Other abbreviations: DMSO–d_6, dimethyl sulfoxide-d_6; FT–IR spectroscopy, Fourier-transform infrared spectroscopy.

2.2. Chemical Synthesis

Schematic representation of the synthetic route adopted to obtain target compounds **4a – 4d** and **7a – 7d** is shown in Scheme 1.

2.2.1. Synthesis of 2-(4-methoxyphenyl) acetohydrazide (3). 2-(4-Methoxyphenyl)acetyl chloride **(2)** was synthesized by reacting 2-(4-methoxyphenyl) acetic acid **(1)** (1 mmol) in the presence of 1,2–dichloroethane (12 mL) solvent with phosphorus oxychloride (0.4 mL) chlorinating agent under reflux for 3 h. Then, the resulting solution was cooled to room temperature and the solvent was removed under reduced pressure to afford compound **2** that was directly used in the next step without further purification. 2-(4-Methoxyphenyl)acetyl chloride **(2)** was dissolved in acetonitrile (80 mL), added dropwise to a solution containing hydrazine hydrate (1 mmol), TEA (0.5 mL), acetonitrile (20 mL), and allowed to reflux for 3 h with monitoring by TLC. After consumption of the starting material, the reaction mixture was cooled to room temperature. Evaporation of the solvent under reduced pressure yielded crude 2-(4-methoxyphenyl)

acetohydrazide **(3)** as a white solid upon cooling, which was purified by column chromatography when necessary and crystallized from methanol.

2-(4-Methoxyphenyl)acetohydrazide (3): white solid; yield, 86%; MP, 134-136°C; R_f, 0.54 (*n*-hexane – ethyl acetate, 1:1); FT-IR (ν, cm^{-1}): 3334, 3302 (NH_2), 3205 (NH) 3037 (sp^2 CH), 2958, 2837 (sp^3 CH), 1618 (C=O), 1541, 1511, 1497 (C=C of phenyl ring); ^{1}H NMR (400 MHz, DMSO-d_6; δ, ppm): 9.21 (s, 1H, NH), 7.19 (aromatic, d, 2H, *J* = 8.4 Hz), 6.86 (aromatic, d, 2H, *J* = 8.4 Hz), 4.23 (s, 2H, broad, NH_2), 3.71 (s, 3H, OCH_3), 3.28 (s, 2H, CH_2); ^{13}C NMR (100 MHz, DMSO-d_6; δ, ppm): 170.7, 159.6, 143.2, 129.7, 120.8, 114.6, 111.7, 55.3, 35.4.

2.2.2. General procedure for the synthesis of Schiff base derivatives (4a – 4d). 2-(4-Methoxyphenyl) acetohydrazide **3** (0.125 mol, 1 eq) was dissolved in methanol (20 mL) and various substituted aldehydes (0.125 mol, 1 eq) were separately dissolved in methanol (20 mL). The two solutions were mixed together prior to exposure under microwave irradiation for 10 min with constant monitoring the reaction progress by TLC after regular 2-min intervals. On complete consumption of starting materials, the reaction mixture was evaporated at reduced pressure and crystallized from methanol. The product was purified when necessary by column chromatography with *n*-hexane – ethyl acetate solvent system.

(*E*)-*N*′-(Ferrocenylmethylene)-2-(4-methoxyphenyl)-acetohydrazide (4a): dark-brown solid; yield, 86%; R_f, 0.52 (chloroform – methanol, 9:1); IR (ν, cm^{-1}): 3202 (NH), 3062, 2958 (CH), 1677 (C=O), 1602 (C=N), 1547, 1494 (C=C); ^{1}H NMR (400 M Hz, DMSO-d_6; δ, ppm): 10.16 (s, 1H, imine), 8.99 (s, 1H, broad signal, NH), 7.37 – 7.22 (m, 2H, aromatic), 6.90 – 6.89 (m, 2H, aromatic), 4.82 – 4.01 (m, 9H, ferrocene), 3.65 (s, 2H, aliphatic CH_2), 3.62 (s, 3H, methoxy); ^{13}C NMR (100 MHz, DMSO-d_6; δ, ppm): 171.1, 158.9, 145.2, 130.6, 127.3, 78.5, 77.4, 76.8, 73.2, 70.6, 69.3, 68.1, 67.7, 60.4, 55.2, 38.9.

(*E*)-*N*′-[{2,3-Dihydrobenzo(b](1,4)dioxin-6-yl}methylene]-2-(4-ethoxyphenyl) acetohydrazide (4b): off-white solid; yield, 85%; R_f: 0.53 (chloroform – methanol, 9:1); IR (ν, cm^{-1}): 3203 (NH), 3087, 3011 (CH), 1663 (C=O), 1601 (C=N), 1548, 1493 (C=C); ^{1}H NMR (400 M Hz, DMSO-d_6; δ, ppm): 10.03 (s, 1H, imine), 8.70 (s, 1H, broad signal, NH), 7.89 (s, 1H, aromatic), 7.69 (d, 1H, J = 7.5, aromatic), 7.43 (d, 1H, J = 7.5, aromatic), 7.32 – 7.22 (m, 1H, aromatic), 7.19 – 7.14 (m, 1H, aromatic), 6.92 – 6.85 (m, 2H, aromatic), 4.36 (t, 2H, aliphatic), 4.27 (t, 2H, aliphatic), 3.64 (s, 2H, aliphatic CH_2), 3.65 (s, 3H, methoxy); ^{13}C NMR (100 MHz, DMSO-d_6; δ, ppm): 174.2, 158.5, 147.8, 145.5, 143.8, 130.5, 127.5, 125.9, 121.4, 117.5, 115.6, 114.2, 64.5, 64.1, 55.3, 38.5.

(*E*)-*N*′-[Benzo(b)thiophen-2-ylmethylene]-2-(4-methoxyphenyl) acetohydrazide (4c): yellow solid; yield, 85%; R_f, 0.50 (chloroform – methanol, 9:1); IR (ν, cm^{-1}): 3203 (NH), 3058, 2928 (CH), 1663 (C=O), 1603 (C=N), 1548, 1494 (C=C); ^{1}H NMR (400 M Hz, DMSO-d_6; δ, ppm): 10.13 (s, 1H, imine), 8.77 (s, 1H, broad signal, NH), 7.84 – 7.79 (m, 2H, aromatic), 7.71 (s, 1H, thiophene), 7.67 – 7.51 (m, 2H, aromatic), 7.36 – 7.21 (m, 2H, aromatic), 6.97 – 6.85 (m, 2H, aromatic), 3.65 (s, 2H, aliphatic CH_2), 3.71 (s, 3H, methoxy); ^{13}C NMR (100 MHz, DMSO-d_6; δ, ppm): 171.4, 159.1, 146.2, 138.4, 136.5, 135.4, 132.3, 130.1, 127.5, 127.2, 126.5, 122.7, 119.1, 114.9, 56.1, 38.8.

(*E*)-*N*′-[(2,2′-Bithiophen-5-yl)-methylene]-2-(4-methoxyphenyl) acetohydrazide (4d): light-brown solid; yield, 88%; R_f, 0.50 (chloroform – methanol, 9:1); IR (ν, cm^{-1}): 3202 (NH), 3064, 2934 (CH), 1663 (C=O), 1592 (C=N), 1549, 1513, 1494 (C=C); ^{1}H NMR (400 M Hz, DMSO-d_6; δ, ppm): 10.10 (s, 1H, imine), 8.87 (s, 1H, broad signal, NH), 7.85 – 7.76 (m, 2H, aromatic), 7.73 – 7.71 (m, 2H, aromatic), 7.35 – 7.31 (m, 2H, aromatic), 7.24 – 7.18 (m, 2H, aromatic), 7.14 – 7.09 (m, 2H, aromatic), 6.96 – 6.87 (m, 2H, aromatic), 3.65 (s, 2H, aliphatic CH_2), 3.74 (s, 3H, methoxy); ^{13}C NMR (100 MHz, DMSO-d_6; δ, ppm): 171.8, 159.0, 143.9, 136.7, 131.4, 129.7, 127.4, 126.5, 126.1, 122.3, 121.4, 119.7, 115.2, 114.3, 55.4, 38.6.

2.2.3. Synthesis of 4-amino-3-(4-methoxybenzyl)-1*H*-1,2,4-triazole-5(4*H*)thione (6). To potassium hydroxide (0.125 mol) dissolved in dry methanol (50 mL) was added 2-(4-methoxyphenyl) acetohydrazide **(3)** (0.125 mol) and the solution was cooled on ice. To this, solution was slowly added carbon disulfide (0.125 mol) in small portions with constant stirring for 2–3 h. The solid product of potassium 2-[2-(4-methoxyphenyl)acetyl]hydrazinecarbodithioate **(5)** was filtered, washed with chilled diethyl ether, and dried. It was directly used in the next step without purification. To potassium 2-[2-(4-methoxyphenyl)acetyl]hydrazine carbodithioate **(5)** in deionized water (20 mL) was added hydrazine hydrate (0.250 mol) and the mixture was refluxed for 8 – 10 h. The reaction mixture turned yellowish-green with evolution of hydrogen sulfide and finally it became homogeneous. Then, the mixture was poured in crushed ice and neutralized with hydrochloric acid. The white precipitate of 4-amino-3-(4-methoxybenzyl)-1*H*-1,2,4-triazole-5(4*H*)thione **(6)** was filtered, washed with cold water, and crystallized from aqueous methanol.

4-Amino-3-(4-methoxyphenyl)-1*H*-1,2,4-triazole-5(4*H*)-thione (6): white solid; yield, 75%; MP, 215 – 217°C; R_f, 0.71 (petroleum ether – ethyl acetate, 7:3); IR (ν, cm^{-1}): 3294, 3130 (NH), 3350 – 3273 (NH_2), 2937 (sp^2 CH), 1585 (C=N), 1561 – 1506 (C=C), 1335 (C=S); ^{1}H NMR (400 MHz, $CDCl_3$; δ, ppm): 13.81 (s, 1H, NH), 7.98 – 7.95 (m, 2H, Ar-H), 7.07 – 6.97 (m, 2H, Ar-H), 5.76 (s, 2H, NH_2), 3.72 (s, 3H, OCH_3); ^{13}C NMR (100 MHz, $CDCl_3$; δ, ppm): 167.12, 161.31, 158.22, 132.57, 130.11, 118.61, 56.32.

2.2.4. General procedure for the synthesis of Schiff base derivatives (7a – 7d). 4-amino-3-(4-methoxybenzyl)-

1*H*-1,2,4-triazole-5(4*H*)thione **(6)** (0.125 mol, 1 eq) was dissolved in methanol (20 mL) and various substituted aldehydes (0.125 mol, 1 eq) were separately dissolved in methanol (20 mL). The two solutions were mixed together prior to exposure under microwave irradiation for 10 min with constant monitoring of the reaction progress by TLC at regular 2-min intervals. Upon complete consumption of starting materials, the reaction mixture was evaporated at reduced pressure and crystallized from methanol. The product was purified when necessary by column chromatography with *n*-hexane – ethyl acetate solvent system on needed.

(*Z*)-4-{(ferrocenylmethylene)amino}-3-(4-methoxybenzyl)-1*H*-1,2,4-triazole-5(4*H*)thione (7a): dark-brown solid; yield, 86%; R_f, 0.54 (chloroform – methanol, 9:1); IR (ν, cm^{-1}): 3079, 2977 (CH), 1588 (C=N), 1561, 1544, 1479 (C=C), 1329 (C=S); ^{1}H NMR (400 M Hz, DMSO-d_6); δ, ppm): 13.88 (s, 1H, broad, NH), 10.16 (s, 1H, imine), 7.24 – 7.18 (m, 2H, aromatic), 6.98 – 6.87 (m, 2H, aromatic), 4.84 – 4.06 (m, 9H, ferrocene), 3.56 (s, 2H, aliphatic CH_2), 3.54 (s, 3H, methoxy); ^{13}C NMR (100 MHz, DMSO-d_6; δ, ppm): 162.1, 159.6, 157.7, 149.5, 132.9, 124.9, 122.3, 77.6, 77.3, 75.8, 73.2, 70.5, 68.9, 68.1, 60.3, 55.5, 38.6.

(*Z*)-4-[{(2,3-dihydrobenzo[*b*][1,4]dioxin-6-yl)methylene}amino]-3-(4-methoxybenzyl)-1*H*-1,2,4-triazole-5(4*H*)-thione (7b): yellow solid; yield, 85%; R_f, 0.51 (chloroform – methanol, 9:1); IR (ν, cm^{-1}): 3094, 2981 (CH), 1597 (C=N), 1561, 1527, 1487 (C=C), 1329 (C=S); ^{1}H NMR (400 M Hz, DMSO-d_6; δ, ppm): 13.89 (s, 1H, broad, NH), 10.04 (s, 1H, imine), 7.94 – 7.91 (m, 1H, aromatic), 7.51 – 7.47 (m, 1H, aromatic), 7.27 – 7.18 (m, 2H, aromatic), 6.96 – 6.88 (m, 3H, aromatic), 4.29 (t, 2H, aliphatic), 4.29 (t, 2H, aliphatic), 3.59 (s, 2H, aliphatic CH_2), 3.55 (s, 3H, methoxy); ^{13}C NMR (100 MHz, DMSO-d_6; δ, ppm): 162.9, 159.4, 157.5, 154.6, 149.5, 149.2, 136.5, 132.0, 129.5, 128.6, 121.5, 118.2, 115.4, 65.3, 65.1, 55.6, 38.3.

(*Z*)-4-{(benzo[*b*]thiophen-2-ylmethylene)amino}-3-(4-methoxybenzyl)-1*H*-1,2,4-triazole-5(4*H*)thione (7c): beige solid; yield, 85%; R_f, 0.52 (chloroform – methanol, 9:1); IR (ν, cm^{-1}): 3070, 2961, 2833 (CH), 1587 (C=N), 1584, 1452 (C=C), 1331 (C=S); ^{1}H NMR (400 M Hz, DMSO-d_6; δ, ppm): 13.85 (s, 1H, broad, NH), 10.12 (s, 1H, imine), 7.88 – 7.77 (m, 2H, aromatic), 7.64 – 7.53 (m, 3H, aromatic), 7.34 – 7.23 (m, 2H, aromatic), 7.97 – 7.84 (m, 2H, aromatic), 3.59 (s, 2H, aliphatic CH_2), 3.67 (s, 3H, methoxy); ^{13}C NMR (100 MHz, DMSO-d_6; δ, ppm): 165.5, 159.3, 158.2, 149.8, 137.1, 136.5, 134.4, 131.3, 129.2, 126.3, 122.4, 122.3, 118.7, 115.9, 55.8, 38.9.

(*Z*)-4-[{(2,2′-bithiophen)-5-ylmethylene}amino]-3-(4-methoxybenzyl)-1*H*-1,2,4-triazole-5(4*H*)thione (7d): mustard solid; yield, 87%; R_f, 0.54 (chloroform – methanol, 9:1); IR (ν, cm^{-1}): 3078, 2954 (CH), 1592 (C=N), 1554, 1533, 1478 (C=C), 1334 (C=S); ^{1}H NMR (400 M Hz, DMSO-d_6; δ, ppm): 13.81 (s, 1H, broad, NH), 10.14 (s, 1H, imine), 7.81 – 7.64 (m, 2H, aromatic), 7.34 – 7.11 (m, 5H, aromatic), 6.97 – 6.89 (m, 2H, aromatic), 3.58 (s, 2H, aliphatic CH_2), 3.67 (s, 3H, methoxy); ^{13}C NMR (100 MHz, DMSO-d_6; δ, ppm): 164.5, 159.6, 157.8, 149.5, 144.5, 137.8, 136.4, 135.5, 131.1, 129.4, 128.3, 122.4, 119.8, 118.1, 114.5, 55.5, 38.4.

2.3. Biological Activity

2.3.1. *In vivo* anti-inflammatory activity protocol. Anti-inflammatory activity of synthetic compounds was evaluated using the carrageenan induced rat paw edema test by following the reported procedure [23, 24].

Animals and maintenance. Healthy adult male Sprague – Dawley rats (n = 50, average body weight 150 ± 10 g) were obtained from the Daehan Biolink Co. (Chungcheongbuk-Do, Korea). Five animals were housed per cage. They were maintained at standard conditions of laboratory temperature and photoperiod and had free access to standard rodent diet.

Dosage. 1% (w/v) solution of lambda carrageenan (Sigma) was prepared in 0.9 % saline. The model edema was induced by injecting 0.1 mL carrageenan solution. Standard drug indomethacin (Sigma) was injected at 10 mg/kg only to animals in the positive control group. Test compounds were injected at a dose of 5 mg/animal.

Experimental design. Rats were weighed and marked with individual numbers. Weighed rats were divided into ten groups, each group containing five animals as follows:

(i) normal control group treated with standard drug indomethacin;

(ii) positive control (carrageenan edema) group pretreated with standard drug indomethacin; (iii – vi) carrageenan edema test groups pretreated with compounds **4a, 4b, 4c,** and **4d,** respectively;

(vii – x) carrageenan edema test groups pretreated with compounds **7a, 7b, 7c,** and **7d,** respectively.

One hour after injecting test compounds or standard drug, the edema model was induced in the rat paw by injecting 0.1 mL of freshly prepared 1% w/v carrageenan solution into subplantar tissues of the left hind paw of each rat. The paw volume of the rat was determined instantaneously after the carrangeenan injection (0 h) and then at every 1 h interval for 7 h by the volume displacement method using digital plethysmometer (Ugo Basile, 21025 Comerio (VA), Italy). The percentage inhibition of edema was calculated using the following formula:

$$\text{Percentage edema inhibition} = \frac{\text{N.C} - \text{C.E}}{\text{N.C}} \times 100,$$

where N. C is the mean increase in paw volume of negative control and C. E is the mean increase in paw volume of compound treated or positive group.

Statistical Analysis. Experimental data were analyzed through one-way analysis of variance (ANOVA) using the Statistical Package for Social Sciences (SPSS version 16.0

Inc. Chicago, Illinois, USA). $P < 0.05$ was considered statistically significant difference.

2.3.2. Free radical scavenging assay protocol. Free radical scavenging activity of the synthesized compounds were determined by 2,2-diphenyl-1-picrylhydrazyl (DPPH) assay following the reported procedure [25 – 28]. Briefly, the assay solution consisted of 100 μL of 150 μM DPPH and 20 μL of increasing concentration of test compound, with the total volume adjusted to 200 μL with DMSO in each well. The reaction mixtures were then incubated for 30 min at room temperature. Ascorbic acid (vitamin C) was used as the reference drug. The assay measurements were carried out for 96-well plates using a microplate reader (OPTI $_{Max}$, Tunable Micro Plate Reader; wavelength range, 340 – 850 nm) at 517 nm. The reaction rates of test compounds were compared to the reference drug and the percentage inhibition was calculated as $100 - (Abs_{test}/Abs_{control}) \times 100$, where Abs is the peak absorbance [29]. Each concentration was analyzed in three independent experimental runs in triplicate. The IC_{50} values were determined by the data analysis and graphing 64-bit Origin 8.6 software.

2.4. Computational Methodology

2.4.1. Retrieval of protein structures from PDB. COX-1 and COX-2 receptors were used to identify the binding affinity of synthesized ligands. In our experimental study we analyzed the inflammatory activity, therefore, both COX-1 and COX-2 were accessed and used as target molecules. Preliminary results showed that both structures could be used to predict anti-inflammatory activity [30]. Both target proteins (COX-1 and COX-2) were accessed through homology based modeling and Protein Data Bank. The crystal structure of human COX-1 is not present in PDB [31, 32]. Therefore, homology modeling approach was employed to predict three-dimensional (3D) structure of COX-1 protein. The amino acid sequences of COX-1 in FASTA format having accession number (P23219) was obtained from Uniprot Knowledge database (http://www.uniprot.org/). To build COX-1 model, the Swiss modeling approach was employed using sheep (*Ovis aries*) template having PDBID 401Z on the basis of sequence identity 92.97% and query coverage 31 – 583 amino acids. The crystal structure of human COX-2 was retrieved from the PDB with PDBID 5F19. Furthermore, the validity of predicted structure was confirmed using various evaluation tools such as ERRAT, Anolea, ProCheck, and Rampage [33 – 36]. Energy minimization of COX-1 was performed through Vega-ZZ [37] while UCSF Chimera 1.6 was employed to visualize the predicted structures [38]. The overall stereo-chemical properties, hydrophobicity, and Ramachandran values of COX-1 and COX-2 were assessed using Discovery Studio 4.0 and MolProbity server, respectively [39, 40].

2.4.2. Computational design of synthesized ligands. The synthesized compounds **7a** – **7d** were sketched in drawing ACD/ChemSketch tool and minimized by UCSF Chimera 1.10.1. The Molsoft (http://www.molsoft.com/) and Molinspiration (http://www.molinspiration.com/) online ligand analysis tools were employed to predict the drug-likeness and basic biological properties of these designed structures. Moreover, Lipinski's rule of five (RO5) was analyzed using Molsoft and Molinspiraion tools. The numbers of rotatable bonds, H-bond acceptors (HBA), and H-bond donors (HBD) were also confirmed by PubChem (https://pubchem.ncbi.nlm.nih.gov/). The pharmacokinetic properties like Absorption, Distribution, Metabolism, Excretion and Toxicity (ADMET) were evaluated using pkCSM server [41].

2.4.3. Grid generation and molecular docking using PyRx tool. Prior to molecular docking, the optimized COX-1 and COX-2 structures were prepared. Bond orders were assigned and hydrogen atoms were added to the protein. Grid preparation and molecular docking study was carried out for the synthesized ligands **7a** – **7d** against COX-1 and COX-2 to obtain different docked complexes by PyRx tool (Vina Wizard) [42]. The grid box parametric values of $X = 28.6432$, $Y = 28.6975$, and $Z = 9.4725$ with 1.0 Å spacing, and exhaustiveness values (8) were adjusted to attain the finest binding conformational pose of ligands. Molecular docking approach was employed for all ligands (**7a** – **7d**) against COX-1 and COX-2 to obtain various docked complexes. Furthermore, the obtained COX1 and COX-2 docked complexes were further evaluated on lowest binding energy (kcal/mol) values and ligand – protein binding interaction patterns (hydrogen/hydrophobic). Docking analysis was employed by Discovery Studio (2.1.0) and UCSF Chimera 1.10.1.

3. RESULTS AND DISCUSSION

3.1. Chemistry

The conversion of 2-(4-methoxyphenyl)acetic acid **(1)** to 2-(4-methoxyphenyl)acetyl chloride **(2)** was indicated by IR spectral data as the disappearance of broad signal in the range of 3400 – 2500 cm^{-1} related to acid hydroxyl group. The formation of 2-(4-methoxyphenyl)acetohydrazide **(3)** was indicated by IR spectral data as the appearance of new peaks at 3334 and 3302 – 3205 cm^{-1} related to primary and secondary amino group of acid hydrazide. In addition, there was a slight shift in the carbonyl stretching vibrations from 1733 to 1618 cm^{-1} indicating the successful conversion of 2-(4-methoxyphenyl)acetyl chloride **(2)** into 2-(4-methoxyphenyl)acetohydrazide **(3)**. The appearance of a broad singlet at 9.21 ppm due to primary NH proton resolution as well as 4.23 ppm due to secondary NH proton resolution further confirmed the formation of 2-(4-methoxyphenyl) acetohydrazide **(3)**. The transformation of 2-(4-methoxyphenyl) acetohydrazide **(3)** into substituted Schiff base derivatives **4a – 4d** was initially indicated by the FT-IR spectral data as the appearance of new signals in the range of 1603 – 1592 cm^{-1} related to C=N stretching vibrations and

complete decline in NH_2 peak of bare hydrazide moiety. Further confirmation of target Schiff base derivatives **4a – 4d** was based on ^{1}H NMR and ^{13}C NMR spectral analysis. The appearance of downfield singlet peak in case of ^{1}H NMR spectra in the range of 10.13 – 10.03 ppm due to imine proton and disappearance of NH_2 signal at 4.23 ppm confirm the formation of target compounds **4a – 4d**. Further evidence about product formation was obtained from ^{13}C NMR spectral analysis. The formation of 4-amino-3-(4-methoxybenzyl)-1*H*-1,2,4-triazole-5(4*H*)-thione **(6)** was confirmed by IR, ^{1}H NMR and ^{13}C NMR spectral analysis. In the IR spectrum, a relatively broad peak in the range of 3294 – 3130 cm^{-1} with shoulder for NH_2 stretching vibration and a new signal at 1335 cm^{-1} for C=S stretching vibration were observed, which indicated the transformation of 2-(4-methoxyphenyl)acetohydrazide **(3)** into 4-amino-3-(4-methoxybenzyl)-1*H*-1,2,4-triazole-5(4*H*)-thione **(6)**. In the ^{1}H NMR, the presence of characteristic highly downfield signal at 13.81 ppm due to triazole ring secondary amino proton and disappearance of secondary amino proton confirmed the formation of 4-amino-3-(4-methoxybenzyl)-1*H*-1,2,4-triazole-5(4*H*)-thione **(6)**. The condensation of 4-amino-3-(4-methoxybenzyl)-1*H*-1,2,4-triazole-5(4*H*)-thione **(6)** with various substituted aldehydes was confirmed by NMR (^{1}H NMR and ^{13}C NMR) spectral analysis and FT-IR spectroscopy. The FT-IR spectrum indicated the formation of target compounds **7a – 7d** by the disappearance of relatively broad peak in the range of 3280 – 3169 cm^{-1} with shoulder for NH_2 stretching vibration. The NMR spectra provide further confirmation about successful condensation of different substituted aldehydes with the 4-amino-3-(4-methoxybenzyl)-1*H*-1,2,4-triazole-5(4*H*)-thione **(6)** through the disappearance of broad signal in the range of 3.59 – 3.56 ppm and the appearance of new downfield signal in the range of 10.16 – 10.04 ppm due to imine proton resolution. Furthermore, there was a slight shift in the triazole NH signal in the ^{1}H NMR spectra of the resulting compounds alongside with the additional signals in both carbon and proton NMR spectra, which confirmed the successful synthesis of target compounds **7a – 7d**.

3.2. Pharmacology

3.2.1. *In vivo* anti-inflammatory activity. In this study, eight compounds (**4a – 4d** and **7a – 7d)** were tested on rats for anti-inflammatory potential. In general, the animals remained healthy and active, and no any deaths occurred in any group. Compound **4a** showed significantly lowered volume of rat paw edema ($P < 0.05$; Fig. 1A). Compound **4b** did not show significant anti-inflammatory activity (Fig. 1B). Highly significant anti-inflammatory activity was observed for compound **4c** ($P < 0.05$; Fig. 1C), whereas compound **4d** was not significantly active against inflammation (Fig. 1D). Meanwhile, compound **7a** showed highly momentous percentage inhibition of rat paw edema volume ($P < 0.05$; Fig. 1E), while no significant change was observed for compound **7b** (Fig. 1F). Injection of compound **7c** appreciably lowered the edema volume ($P < 0.05$; Fig. 1G). Compound **7d** caused no any notable change in edema volume (Fig. 1H). It appears from the present study that compounds **4a**, **4c**, **7a** and **7c** exhibited almost similar activities in increasing percentage inhibition of rat paw edema. Compounds **4a** and **7a** contain ferrocenyl group as substituent R, while in case of compounds **4c** and **7c** there is 2-methylbenzo[*b*]thiophenyl group as substituent R. Meanwhile, compounds **4b**, **4d**, **7b** and **7d** did not show any significant anti-inflammatory activity. In case of **4b** and **7b**, there was 6-methyl-2,3-dihydrobenzo[*b*][1, 4]dioxinyl group as substituent R, while compounds **4d** and **7d** have 5-methyl-2,2′-bithiophenyl group as substituent R. From these results, it was concluded that isolated thiophenyl group attached through Schiff base formation in the core skeleton of the target compounds caused suppression of anti-inflammatory potential, while in bicyclic system with phenyl ring, this group caused increase in anti-inflammatory activity. Meantime, dioxane moiety in connection to phenyl ring as bicyclic system reduced the anti-inflammatory potential of Schiff base derivatives (Fig. 1).

In conclusion, the results showed considerable variation in biological activity of the synthesized compounds depending on changes in their structures. The aralkyl moiety in the target compounds **4a – 4d** and **7a – 7d** did not exert much effect on the anti-inflammatory potential of the synthesized Schiff base derivatives. On the other hand, a change in substituent R led to considerable alteration in the biological activity. The ferrocenyl group and 2-methylbenzo[*b*]thiophenyl were found to be excellent candidates to incorporate the anti-inflammatory potential in the synthesized Schiff base derivatives **4a – 4d** and **7a – 7d**.

3.2.2. Anti-oxidant activity. In the DPPH free radical scavenging assay, ascorbic acid with IC_{50} 2.61 ± 0.29 μg/mL was used as the standard drug. Compound **7a** with IC_{50} value of 7.2 ± 2.7 μg/mL was the most active compound among the series studied, while the IC_{50} values of other synthesized compounds was in the range of 330.2 ± 10, 172.4 ± 4 and 403.4 ± 7 μg/mL for **7b**, **7c** and **7d**, respectively. In case of the synthesized Schiff base derivatives **4a – 4d**, no significant anti-oxidant potential was found. These results lead us to conclude that the Schiff base derivatives containing 3,4-disubstitued 1,2,4-triazole nucleus exhibit considerable anti-oxidant potential, while this anti-oxidant activity was not triggered by only triazole subunit, as there were noticeable fluctuations in the DPPH free-radical scavenging assay results for varying side coupled R group. The most potent compound with respect to DPPH free-radical scavenging assay was **7a** exhibiting IC_{50} values almost close to standard drug (vitamin C), which was considered to be due to 3,4-disubstitued 1,2,4-triazole unit as well as substituted ferrocenyl moiety. Meanwhile, the second and third most active compounds among the series were **7c** and **7b** containing 2-methylbenzo[*b*]thiophenyl as well as 6-methyl-2,3-dihydrobenzo[*b*][1, 4]dioxine groups as substituent R along with

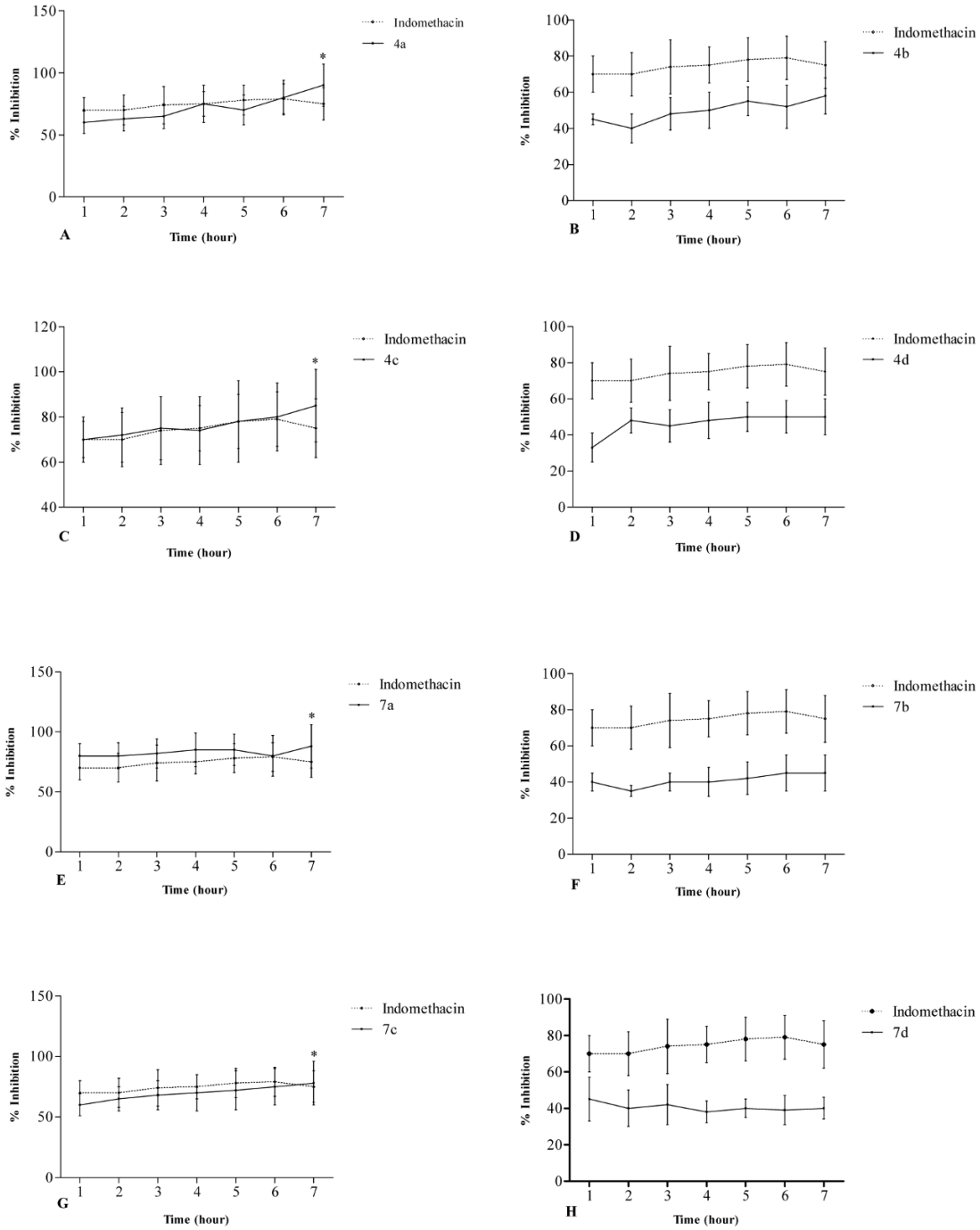

Fig. 1. Percentage inhibition of rat paw edema treated with compounds **4a** (A), **4b** (B), **4c** (C), **4d** (D), **7a** (E), **7b** (F), **7c** (G), **7d** (H) and indomethacin (reference drug, * $P < 0.05$).

side coupled groups. However, the least active compound among synthesized compounds **7a – 7d** was **7d,** which contained 5-methyl-2,2′-bithiopheny as substituent R. Concurrently, there was no anti-oxidant potential in hydrazide substituted Schiff base derivatives **4a – 4d**. The results of anti-oxidant assay for the synthesized compounds **7a –7d** along with control are shown in Fig. 2.

In summary, from these results it was concluded that a side coupled substituent alone exerts negligible effect on the anti-oxidant potential, while in connection through Schiff base formation with 3,4-disubstitued 1,2,4-triazole subunit, it becomes more potent against scavenger during the time and in connection to hydrazide through Schiff base formation it does not implement any scavenging effect.

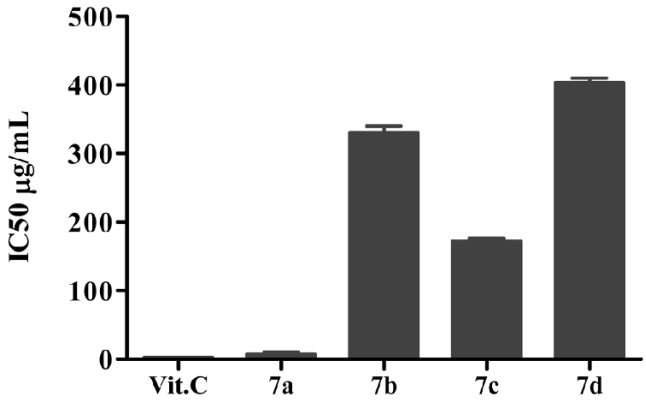

Fig. 2. DPPH free-radical scavenging assay results for synthesized Schiff base derivatives **7a** – **7d** (compounds **4a** – **4d** did not exhibit any scavenging potential at concentrations up to 500 µg/mL).

3.3. Computational Analysis

3.3.1. COX-1 and COX-2 structure evaluation. The COX-1 and COX-2 are functionally involved in prostaglandin (PG). COX-1 contains 599 amino acids, whereas COX-2 consists of 604 residues. Available research data showed that that the crystal structure of COX-1 was not reported; therefore, *in-silico* approach was used to predict 3D structure of COX-1 protein. The reliability and efficacy of both COX-1 and COX-2 structures were analyzed on the basis of Ramachandran and hydrophobicity graphs. The Ramachandran plots of both COX-1 and COX-2 indicate that 95.01% and 97.3% residues, respectively, are present in favorable regions. The generated Ramachandran graphs for COX-1 and COX-2 protein also depicted the good accuracy of phi (ϕ) and psi (ψ) angles among the coordinates, and most of the protein (COX-1 and COX-2) residues are plummeted in the acceptable region. The hydrophobicity graphs for both domains showed residues within the favored region. Moreover, the protein architectures including helices, β-sheets, and coils were also keenly observed through VADAR 1.8 tool. The predicted results show that COX-1 contains 44% helices, 13% β-sheets, and 42% coils, whereas COX-2 comprises 41% helices, 6% β-sheets, and 52% coils. Superimposed structures of both COX-1 and COX-2 with binding pocket are presented in Fig. S1. The hydrophobicity and Ramachandran graphs for COX-1 and COX-2 are shown in Figs. S2 and S3, respectively.

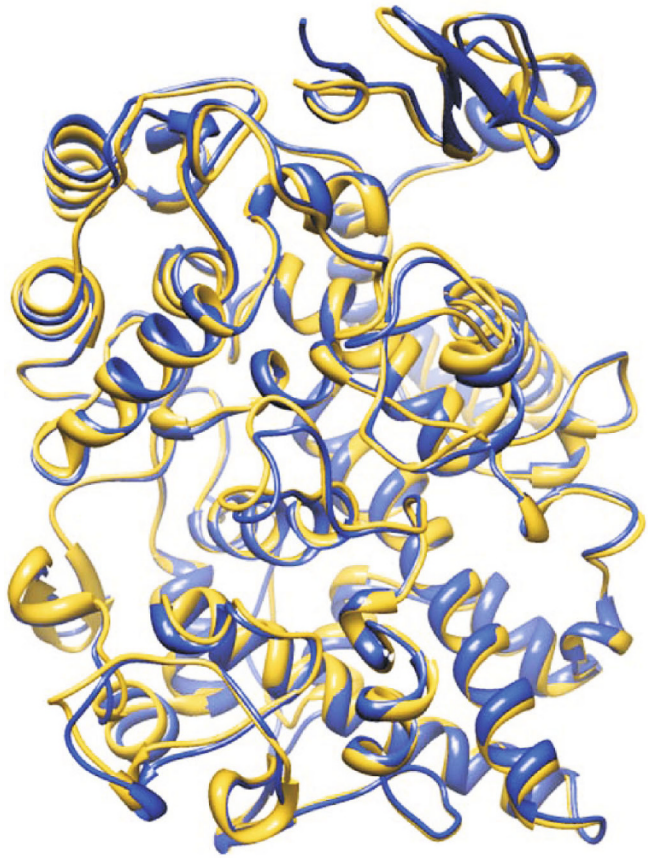

Fig. S1. Superimposed structures of COX-1 (blue) and COX-2 (yellow).

3.3.2. Chemo-informatics evaluation and RO5 analysis of synthesized ligands. Multiple computational servers and tools were used to predict the biochemical properties of synthesized compounds (Table 1). Research data referred to

TABLE 1. Chemo-Informatics Evaluation of Synthesized Compounds

Properties	**7a**	7b	7c	7d
Mol. Weight (g/mol)	458.18	382.11	380.08	412.05
Nunber of HBA	4	6	5	6
Number of HBD	1	1	1	1
Mol. Log*P*	5.95	3.59	4.97	5.45
Number of stereo centers	0	0	0	0
Mol. volume (A^3)	436.13	388.19	383.02	402.18
Drug Likeness Score	0.27	0.06	0.07	0.14

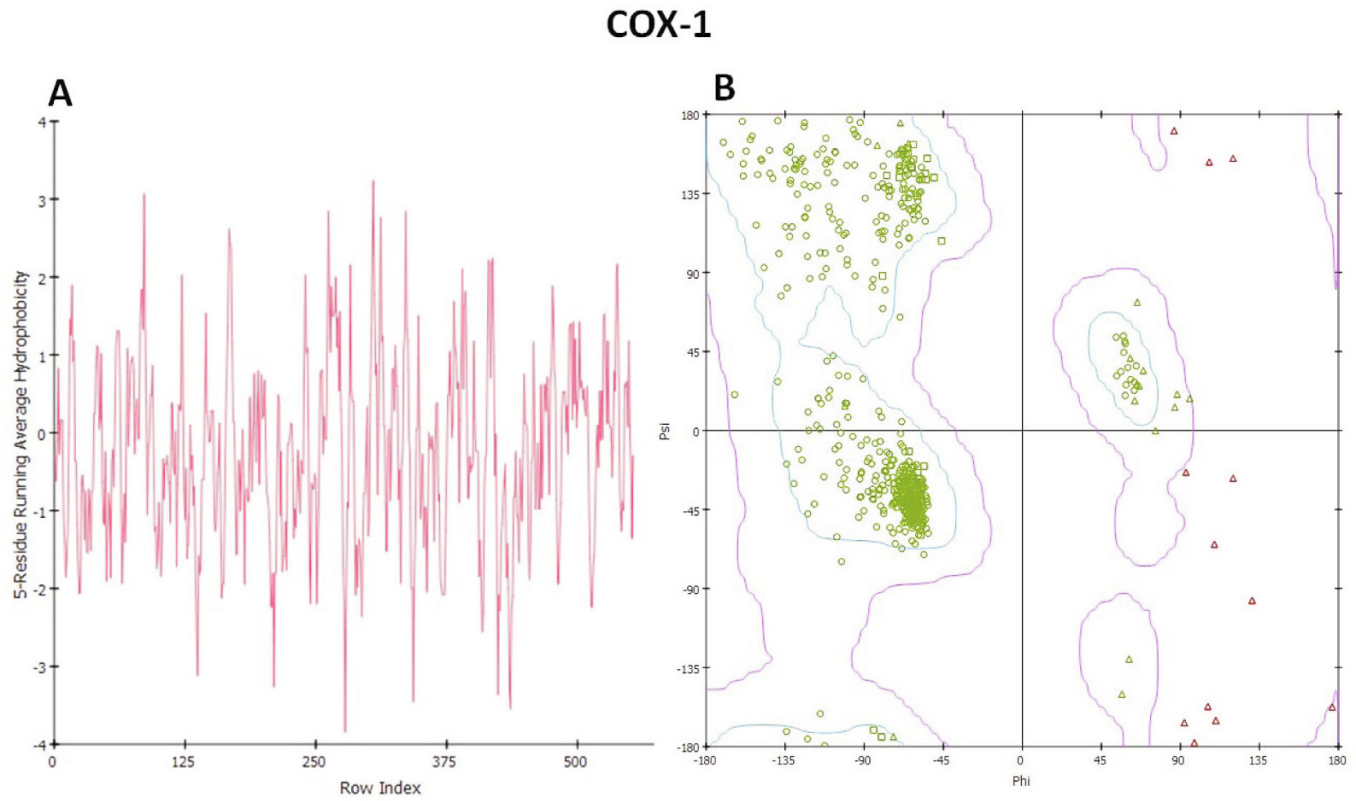

Fig. S2. (**A**) Hydrophobicity and (**B**) Ramachandran graphs of COX-1.

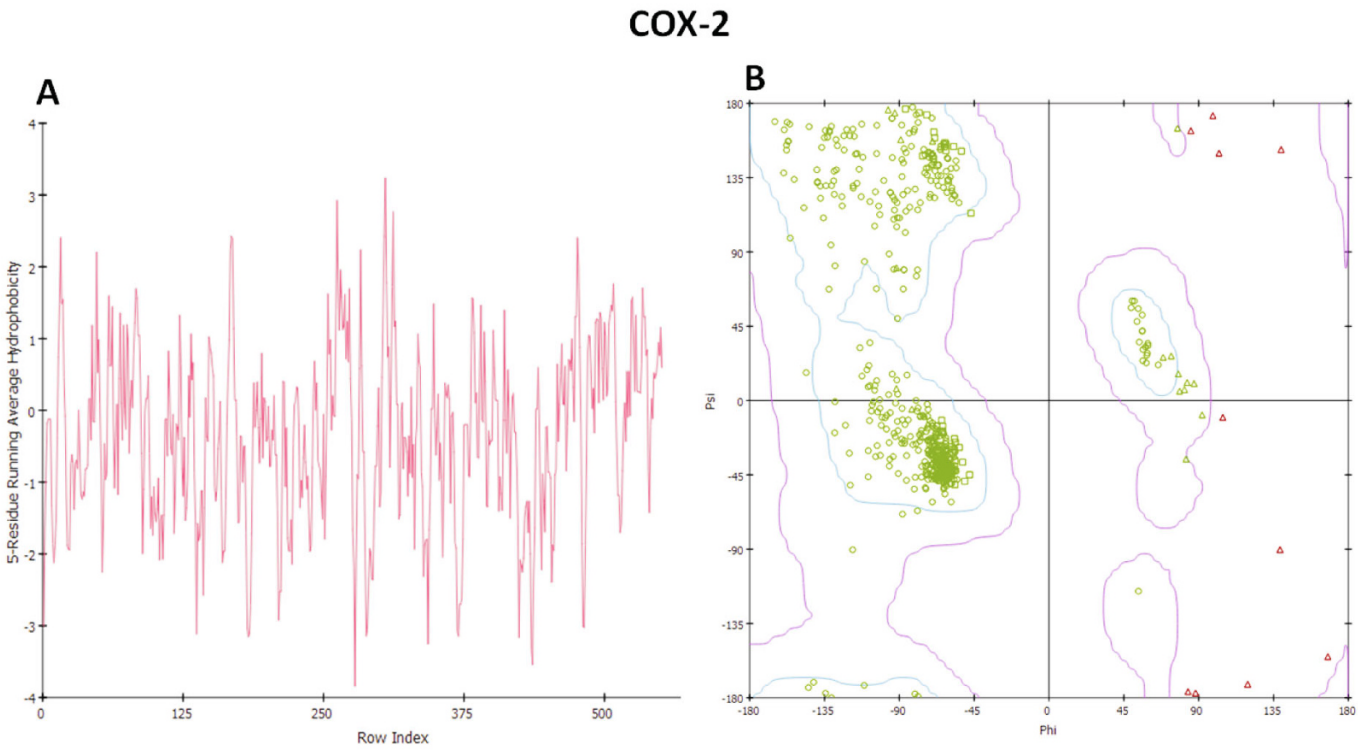

Fig. S3. (**A**) Hydrophobicity and (**B**) Ramachandran graphs of COX-2.

standard values of molecular weight (MW) from 160 to 480 g/mol. Comparative analyses showed that the predicted results for all compounds were comparable with standard values. RO5 analysis also confirmed the therapeutic potential of all ligands. Hydrogen-bonding affinity has also been considered as a significant parameter for evaluating the drug permeability. Some studies showed that excessive values of HBA (>10) and HBD (>5) in ligands resulted in their poor permeation in the body [43, 44]. Our chemo-informatics analyses show that all the designed compounds possess HBA < 10 and HBD < 5, which may confirm their good penetration within the body. Moreover, their log*P* values were also comparable with standard values . However, there are plenty of examples available for RO5 violation among the existing drugs [45 – 47]. The drug score value describes the significance of compounds as lead-like behavior. Results showed that all the compounds may have strong therapeutical potential and potent drug-like behavior. Our *in-silico* depiction for all the compounds agrees with these results.

3.3.3. Pharmacokinetic evaluations of designed compounds. The development of novel drugs requires high attention to their good pharmacokinetic properties. Mostly, ADMET properties assessment is used to confirm the efficacy of results for lead molecules. For calculation of the pharmacokinetic behavior of synthesized ligands (**7a** – **7d**), a freely accessible web server pkCSM was employed to predict their ADMET properties (Table 2). In ADMET evaluation, the predicted values absorption-like aqueous solubility (log mol/L), intestinal absorption (% Abs), and skin permeability (logKp) indicated strong therapeutic potential of selected compounds. It was found that compounds with good absorption have potency to cross the gut barrier by passive penetration to reach the target molecule. The aqueous solubility data showed that compounds **7a** – **7d** had good log mol/L values (–5.296, –3.657, –4.39, and –4.47, respectively). Moreover, the intestinal solubility predictions also justified their good efficacy compared to standard values. The generated results showed that all compounds possess good intestinal solubility values compared to the standard (30% absorption). Compound **7b** showed higher intestinal solubility (92.475% Abs). Investigations showed that compounds with less than 30% Abs value must be considered as poorly absorbed. Furthermore, the skin permeability values (logKp) of all compounds were also greater than standard value (–2.5 logKp) which showed their significance as good lead structures and justified their drug-like behavior. Moreover, blood – brain barrier (BBB) and central nervous system (CNS) permeability values of compounds were also comparable with the standard values (>0.3 and ≤1 logBB; >2 and ≤3 logPS). It has been found that compounds with greater than 0.3 logBB value have potential to cross BBB, while those with less than –1 value are poorly distributed to the brain. Similarly, the ligands having >2 logPS value are considered to penetrate the CNS, while those with ≤3 logPS are difficult to move into the CNS.

The computation generated values for all compounds **7a** – **7d** were comparable with the standard values. Our predicted results showed that selected compounds displayed a significant potential to cross the barriers and may be targeted directly to receptor molecule. Moreover, metabolic behavior with inhibitory potential was confirmed for CYP1A2, CYP2C19, CYP2C9, and CYP3A4. Positive values for all compounds confirmed the strong inhibitory behavior against target proteins with good metabolic behavior. The predicted excretion and toxicity values also justified the drug-like behavior of these compounds on the basis of total clearance (log mL/min/kg), AMES toxicity, maximum tolerated dose (MTD), and LD_{50} values. The AMES toxicity prediction for selected compounds confirmed that there is non-mutagenic and non-toxic behavior. The hepatotoxicity and skin sensitivity negative behavior was showed their non-toxic and less sensitive effects. Compounds **7b** and **7c** showed negative hepatotoxic behavior as compared to other compounds. The absence of skin sensitization effect was observed for all compounds. Thus, hypothetical ADMET properties confirmed that these ligands exhibited good lead-like potential for further evaluation.

TABLE 2. ADMET Assessment of Designed Compounds

ADMET properties*		**7a**	7b	7c	7d
Absorption	WS	-5.296	-3.657	-4.39	-4.47
	IS	83.667	92.475	88.717	87.182
	SP	-2.884	-2.753	-2.738	-2.736
Distribution	VDss	0.306	0.02	-0.374	-0.567
	BBBP	0.211	-1.355	0.222	0.147
	CNSP	-1.585	-2.449	-1.951	-1.958
Metabolism	CYP1A2	Yes	Yes	Yes	Yes
	CYP2C19	Yes	Yes	Yes	Yes
	CYP2C9	Yes	Yes	Yes	Yes
	CYP3A4	Yes	Yes	Yes	Yes
Excretion	TC	-0.032	0.031	0.102	0.055
Toxicity	AMES toxicity	No	No	Yes	Yes
	MTD	-0.308	0.106	0.243	0.287
	ORAT(LD_{50})	2.755	2.476	2.727	2.767
	HT	Yes	Yes	Yes	No
	SS	No	No	No	No

* Abbreviations: WS = water solubility (log mol/L); IS = intestinal solubility (% abs); SP = skin permeability (log Kp); VDss = volumn of distribution (log L/kg); BBBP = blood brain barrier permeability (logBB); CNSP = CNS permeability (logPS); TC = total clearance (log mL/min/kg); MTD = maximum tolerated dose; ORAT = oral rat acute toxicity; HT = hepatotoxicity; SS = skin sensitization.

3.4. Molecular Docking Study

3.4.1. Binding energy analysis. Docking experiments were used only to estimate the binding potential of synthesized ligands against molecular targets (COX1, COX2). The docking (protein – ligand) complexes of all compounds **7a** – **7d** were analyzed individually and evaluated for minimum energy (kcal/mol) values presented in Fig. 3. The energy values justified the binding potential of synthesized compounds against the target proteins. Results showed that the docking complexes of compound **7a** were most active against both receptors (COX-1 and COX-2) with lowest binding energy value (–10.4 and –11.0 kcal/mol, respectively) compared to others compounds. The docking energy values of all docking complexes were calculated using the following equation:

$$\Delta G \text{ binding} = \Delta G \text{ gauss} + \Delta G \text{ repulsion} + \Delta G \text{ hbond} + \\ + \Delta G \text{ hydrophobic} + \Delta G \text{ tors.} \quad (1)$$

Here, ΔG gauss is the attractive term for dispersion of two gaussian functions, ΔG repulsion is the square of the distance if closer than a threshold value, ΔG hbond is the ramp function (also used for interactions with metal ions), ΔG hy-

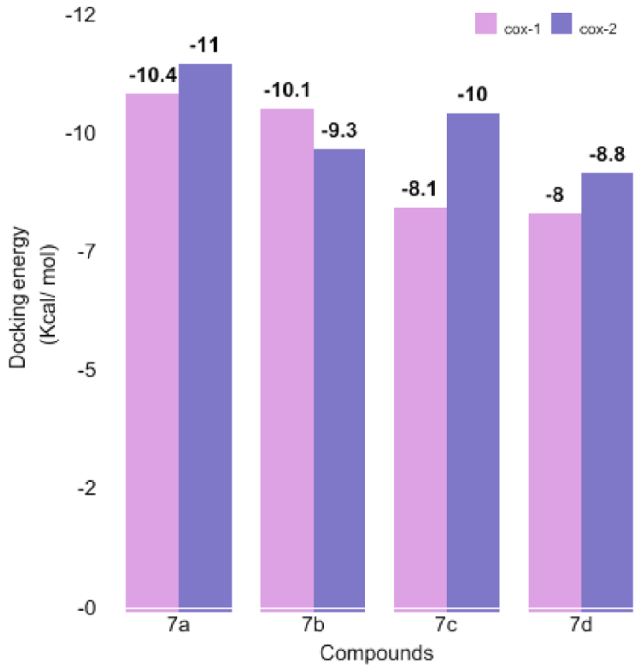

Fig. 3. Docking energy values of synthesized compounds against COX-1 and COX-2**.**

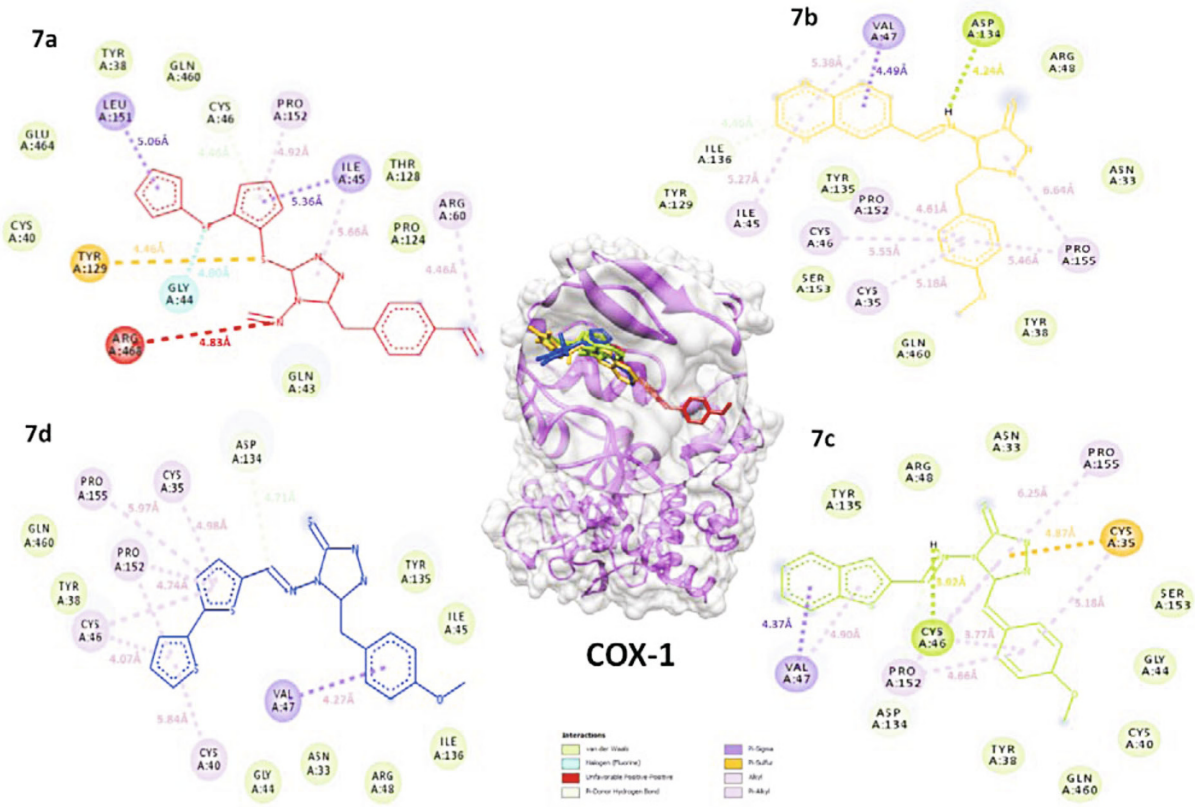

Fig. 4. Docking interactions of compounds **7a** – **7d** with COX-1 enzyme. COX-1 is highlighted in purple color in wire ribbon and surface format with all the four compounds embedded in the middle of diagrams. In detailed interaction patterns against COX-1, ligands **7a** – **7d** are shown in red, yellow, green, and blue color, respectively.

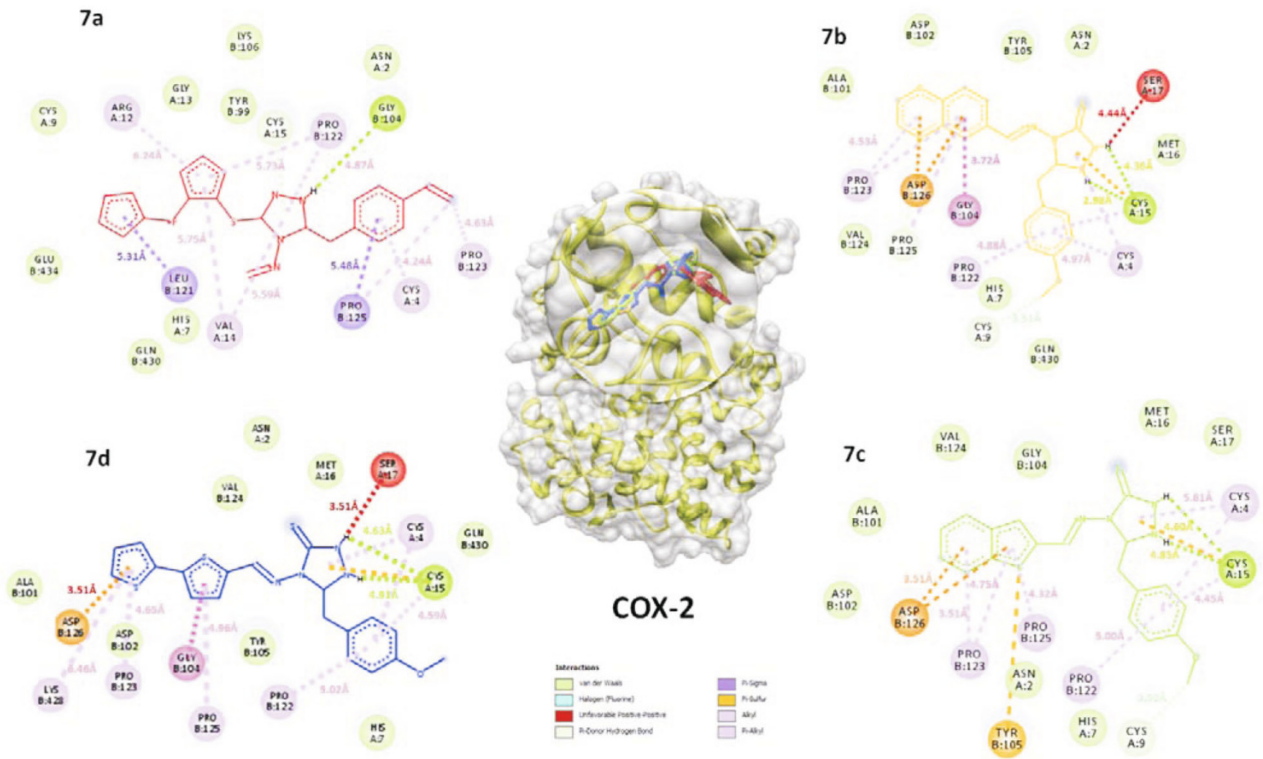

Fig. 5. Docking interactions of compounds **7a** – **7d** with COX-2 enzyme. COX-2 is highlighted in green color in wire ribbon and surface format with all the four compounds embedded in the middle of diagram. In detailed interactions patterns against COX-2, ligands **7a** – **7d** are shown in red, yellow, green, and blue color, respectively.

drophobic is the ramp function, and ΔG tors is proportional to the number of rotatable bonds. Previous research showed that the standard error for Autodock is about 2.5 kcal/mol. However, the predicted energy values for all docking complexes were less than the standard value. Although the basic nucleus of all the synthesized compounds was similar, most of ligands possessed good effective energy values and had no big energy fluctuations.

3.4.2. Structure – activity relationship analysis of synthesized ligands. Structure activity relationship analysis showed that all compounds **7a – 7d** possessed an active region for target proteins (COX-1 and COX-2). Figure 4 shows that in COX-1 docking a bonding interactions were observed in all docking complexes of compounds **7a – 7d**. Seven hydrophobic interactions against **7a** were observed at different residues such as Leu151, Cys46, Pro152, Ile45, Arg60, Tyr129 and Gly44. However, **7b** interacts with COX-1 with hydrogen and hydrophobic interactions at Asp134, Val47, Ile45, Pro152, Cys46, Cys35 and Pro135, respectively having good bonding distances. Five bonds were observed between **7c** and COX-1 protein. One hydrogen bond was observed at Cys46 with bond length 3.92 Å and four hydrophobic interactions were observed at Pro155, Cys35, Pro152 and Val47. In **7d** docking complex, seven hydrophobic interactions were observed at Asp134, Cys35, Pro155, Pro152, Cys46, Val47 and Cys40. In comparative results, it was found that most of residues were common in the interaction pattern, which may confirm their significance in downstream signaling pathways. In COX-2 docking, compound **7a** forms eight hydrophobic interactions at various residual positions including Gly104, Pro122, Pro125, Cys4, Pro123, Arg12, Leu121, and Val14. However, in **7b** and **7c** docking complexes, Cys15 was the commonly interacting residue involved in hydrogen bonding with bond lengths presented in Fig. 5.

4. CONCLUSION

A series of eight imine derivatives were synthesized through microwave-assisted Schiff base formation and the structures of target compounds were characterized by spectral data. All the synthesized derivatives were screened for their *in vivo* anti-inflammatory as well as *in vitro* anti-oxidant activities using carrageenan induced rat paw edema test and DPPH free-radical scavenging assay, respectively. Furthermore, molecular docking experiments were also performed to check the actual binding affinity of ligands against target proteins. Compounds **4a**, **4c**, **7a,** and **7c** significantly decreased the volume of rat paw edema ($P < 0.05$) and were screened as potent anti-inflammatory drugs among the series. Moreover, docking results of these compounds showed their good binding affinity within the active region of target proteins. It is believed that the synthesized Schiff base deriva-

tives can be used for the development of potent anti-inflammatory and anti-oxidant drugs, with considerable advantages of convenient synthetic strategy ensuring high product yield, short reaction time, and commodious handling.

DECLARATION OF INTERESTS

The authors declare no competing interests. M. Hanif and M. Hassan contributed equally to this manuscript.

REFERENCES

1. R. González, S. Rodríguez, C. Romay, et al., *Pharmacol Res*., **39**(1), 55 – 59 (1999).
2. Y. F. Chen, H. Y. Tsai, and T. S. Wu, *Planta Med*., **61**(1), 2 – 8 (1995).
3. V. Mani, K. Ramasamy, and A. B. A. Majeed, *Food Funct*., **4**(4), 557 – 567 (2013).
4. K Seth, S. K. Garg, Raj Kumar, et al., *Med. Chem. Lett*., **5**(5), 512 – 516 (2014).
5. X. Li, J. Y. Zhang, W. Y. Gao, et al., *J. Agric. Food Chem*., **60**(35), 8738 – 8744 (2012).
6. B. B. Silva, S. M. Alencar, H. Koo, et al, *J. Agric. Food Chem*., **61**(19), 4546 – 4550 (2013).
7. S. Jain, S. Tran, M. A. M. El Gendy, et al., *J. Med. Chem*., **55**(2), 688 – 696 (2012).
8. Y. Fu, H. Zhou, M. Wang, et al., *J. Agric. Food Chem*., **62**(18), 4127 – 4134 (2014).
9. H. Zelová, Z. Hanáková, Z. Èermáková, et al., *J. Nat. Prod*., **77**(6), 1297 – 1303 (2014).
10. R. Dubey, P. Singh, A. K. Singh, et al., *Cryst. Growth Des*., **14**(3), 1347 – 1356 (2014).
11. S. V. Joseph, I. Edirisinghe, and B. M. Burton-Freeman, *J. Agric. Food Chem*., **62**(18), 3886 – 3903 (2014).
12. M. Aursnes, J. E. Tungen, A. Vik, et al., *J. Nat. Prod*., **77**(4), 910 – 916 (2014).
13. L. Haya, I. Osante, A. M. Mainar, et al., *Phys. Chem. Chem. Phys*., **15**(23), 9407 – 9413 (2013).
14. M. Kratchanova, P. Denev, and M. Ciz, *Acta Biochim. Pol*., **57**(2), 229 – 234 (2010).
15. P. Pietta, P. Simonetti, and P. Mauri, *J. Agric. Food Chem*., **46**(11), 4487 – 4490 (1998).
16. A. Djeridanea, M. Yousfia, B. Nadjemi, et al., *Food Chem*., **97**(4), 654 – 660 (2006).
17. S. I. Kim, K. Hyeon, and S. Y. Choi, *Mol. Cell Toxicol*., **6**(3), 279 – 285 (2010).
18. Y. L. Ho, S. S. Huang, J. S. Deng, et al., *Bot. Stud*., **53**(1) 55?66 (2012).
19. W. Chen, W. Ou, L. Wang, et al., *Dalton Trans*., **42**(44), 15678 – 15686 (2013).
20. E. R. Milaeva, D. B. Shpakovsky, Y. A. Gracheva, et al., *Dalton Trans*. **42**(19), 6817 – 6828 (2013).
21. J. Y. Bor, H. Y. Chen, G. C. Yen, et al., *J. Agric. Food Chem*. **54**(5), 1680 – 1686 (2006).
22. W. A. Yehye, N. A. Rahman, O. Saad, et al., *Molecules*, **21**, 847 (2016); doi: 10.3390 / molecules21070847.
23. C. A. Winter, E. A. Risley, and G. W. Nuss, *Proc. Soc. Exp. Biol. Med*., **111** 544 – 547 (1962).
24. O. O. Adeyemi, S. O. Okpo, and O. O. Ogunti, *Fitoterapia*, **73**(5), 375 – 380 (2002).
25. S. A. M. Reddya, J. Mudgala, P. Bansal, et al., *Bioorg. Med. Chem*. **19**(1) 384 – 392 (2011).
26. A. A. Ehab., R. M. Julie., and A. K. Ikhlas, *Bioorg. Med. Chem*. **20**(9), 2784 – 2788 (2012).
27. S. Michael, C. Pascal, M. Patricia, et al., *Bioorg. Chem*.. **36**(3), 133 – 140 (2008).
28. S. Suvarna, K. Krishna, S. Kaushik, et al., *Eur. J. Med. Chem*., **62**, 435 – 442 (2013).
29. O. Abid, T. M. Babar, F. Ali, et al., *ACS Med. Chem. Lett*., **1**, 145 – 149 (2010).
30. Z. Ashraf, Alamgeer, R. Rasool., et al., *Int. J. Mol. Sci*., **17**, 2151 (2016).
31. M. N. Marjan, M. T. Hamzeh, E. Rahman, et al., *Comput. Biol. Chem*., **51**, 57 – 62 (2014).
32. Z. Ashraf, Alamgeer, M. Kanwal, et al., *Drug Design, Dev. Ther.*, **10**, 2401 – 2419 (2016).
33. C. Colovos and T. O. Yeates, *Protein Sci.*, **2**(9), 1511 – 1519 (1993).
34. F. Melo, D. Devos, E. Depiereux, et al., *Proc. Int. Conf. Intell. Syst. Mol. Biol*., **5**, 187 – 190 (1997).
35. R. A. Laskowski, M. W. MacArthur, D. S. Moss, et al., *J. Appl. Crystallogr.*, **26**(2), 283–291 (1993).
36. S. C. Lovell, I. W. Davis, W. B. Arendall III, et al., *Proteins*, **50**(3), 437 – 450 (2002).
37. A. Pedretti, L. Villa, and G. Vistoli, *J. Comput. Aided Mol. Des*., **18**(3), 167 – 173 (2004).
38. E. F. Pettersen, T. D. Goddard, C. C. Huang, et al., *J. Comput. Chem*., **25**(13), 1605 – 1612 (2004).
39. *Accelrys Software D Studio, Version 4.1*, Accelrys Software Inc., San Diego, CA (2007).
40. V. B. Chen, W. B. Arendall III, J. J. Headd, et al., *Acta Crystallogr D: Biol Crystallogr.*, **66** (Pt. 1), 12 – 21 (2010).
41. D. E. V. Pires, T. L. Blundell, and D. B. Ascher, *J. Med. Chem*., **58**(9), 4066 – 4072 (2015).
42. S. Dallakyan and A. J. Olson, *Methods Mol. Biol*., **1263**, 243 – 250 (2015).
43. R. U. Kadam and N. Roy, *Indian J. Pharm. Sci*., **69**(5), 609 – 615 (2007).
44. A. K. Ghose, T. Herbertz, R. L. Hudkins, et al., *ACS Chem. Neurosci*., **3**(1), 50 – 68, (2012).
45. M. A. Bakhta, M. S. Yar, S. G. Abdel-Hamid, et al., *Eur. J. Med. Chem*., **45**(12), 5862 – 5869 (2010).
46. S. Tiana, J. Wangc, Y. Li, et al., Adv. *Drug Deliv. Rev.*, **86**, 2 – 10 (2015).
47. P. B. Jadhav, A. R. Yadav, and M. G. Gore, *Int. J. Pharm. Bio. Sci*., **6**, 142 – 154 (2015).